
RCDM: Enabling Robustness for Conditional Diffusion Model

Weifeng Xu

College of Meteorology and Oceanography, National University of Defense Technology
Changsha, CHN 410000
xuweifeng.23@nudt.edu.cn

Xiang Zhu

College of Meteorology and Oceanography, National University of Defense Technology
Changsha, CHN 410000
zhuxiang@nudt.edu.cn

Xiaoyong Li

College of Meteorology and Oceanography, National University of Defense Technology
Changsha, CHN 410000
sayinxmu@nudt.edu.cn

Abstract

The conditional diffusion model (CDM) enhances the standard diffusion model by providing more control, improving the quality and relevance of the outputs, and making the model adaptable to a wider range of complex tasks. However, inaccurate conditional inputs in the inverse process of CDM can easily lead to generating fixed errors in the neural network, which diminishes the adaptability of a well-trained model. The existing methods like data augmentation, adversarial training, robust optimization can improve the robustness, while they often face challenges such as high computational complexity, limited applicability to unknown perturbations, and increased training difficulty. In this paper, we propose a lightweight solution, the Robust Conditional Diffusion Model (RCDM), based on control theory to dynamically reduce the impact of noise and significantly enhance the model's robustness. RCDM leverages the collaborative interaction between two neural networks, along with optimal control strategies derived from control theory, to optimize the weights of two networks during the sampling process. Unlike conventional techniques, RCDM establishes a mathematical relationship between fixed errors and the weights of the two neural networks without incurring additional computational overhead. Extensive experiments were conducted on MNIST and CIFAR-10 datasets, and the results demonstrate the effectiveness and adaptability of our proposed model. Code and project site: https://github.com/*****/RCDM.

1 Introduction

Conditional diffusion models (CDMs) [11, 13, 22] extend traditional diffusion models [20] by integrating additional guidance, such as labels or text, to direct the data generation process. Unlike unguided diffusion generating data through noise addition and denoising, conditional models produce more targeted outputs. These models excel at generating data that matches given criteria, improving accuracy. They are applicable, in handling tasks like computer vision [21, 27, 40], predicting time

series [9, 38], and tackling complex interdisciplinary challenges [41, 48, 51, 52]. Their flexibility and precision make them a powerful tool in diverse domains.

However, conditional diffusion models face severe challenges in real-world scenarios due to noisy data [6, 50]. Neural networks often experience performance degradation in the presence of noise and outliers, which limits their reliability. Robust learning techniques aim to address this issue by enhancing adaptability to data disturbances [3, 37, 46, 49]. The denoising property of diffusion models during the reverse process has been leveraged for adversarial purification [5, 29, 32], partially replacing traditional adversarial training [7, 55, 56], and thus enhancing model robustness. Nevertheless, this approach has limitations when applied to unknown perturbations. Researchers are exploring Distributionally Robust Optimization (DRO) [10, 26, 28] for deeper robustness assurance by considering comprehensive uncertainty in data distributions. However, implementing DRO may require more computational resources. Complementing DRO, enhancing the intrinsic robustness of conditional diffusion models through more resilient model structures can mitigate computational overhead and reduce adversarial example generation, providing inherent resistance to input errors.

This study utilizes the framework of deep reinforcement learning [2, 45], employing the collaborative interaction of two neural networks to enhance model robustness. Concurrently, it incorporates optimal control strategies [47] from control theory, optimizing the weights of the two neural networks through theoretical analysis and validation. Extensive experiments demonstrate the effectiveness and adaptability of our proposals across diverse datasets and network architectures.

2 Related Work

Conditional diffusion models. CDMs [35, 54, 58] are a significant advancement in diffusion models, enabling the generation of data based on specific inputs for greater control over the generative process. CDMs integrates conditioning information into the training process of a neural network, enabling the model to learn the underlying data distribution specific to a given condition (e.g., class label or text description). It allows for controlled data generation during the model’s reverse process. The model consists of two processes, the forward process and the reverse process, as shown in Figure 1. Therefore, CDMs have been applied innovatively to incorporate conditional inputs during neural network training [11, 22, 31]. They utilize unconditional networks to modulate the diversity and relevance of the outcomes, which has been a key aspect of their success. The Denoising Diffusion Probabilistic Models (DDPM) [20, 34, 42] is a prominent research framework for CDMs. It works alongside other frameworks such as score-based generative models (SGM) [43] and stochastic differential equations (SDE) [44], which are interconnected and complementary to each other. Advancements in CDMs have been made through various improvements, including enhancements in neural network architecture [1, 14, 36], efficient sampling [12, 39], likelihood maximization [23, 33], and integration with other generative models [4, 24]. For instance, researchers have worked on scalable architectures, masked autoencoders, and other innovations that have pushed the boundaries of what is possible with these models. These improvements have been documented in various studies, contributing to the ongoing development and refinement of CDMs. The specific mathematical mechanism of CDMs is shown in Appendix A.1.

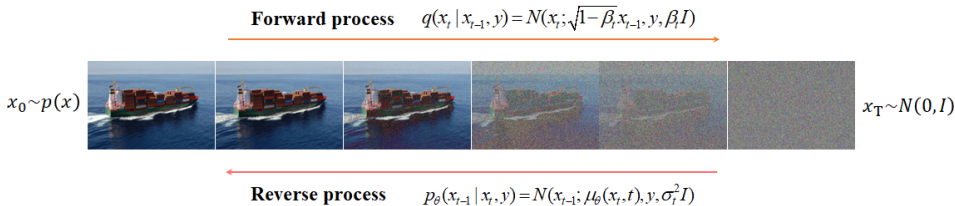


Figure 1: The forward and reverse processes of conditional diffusion models.

Robust learning. In deep learning, model robustness is a critical research goal to enhance their resistance against input disturbances, noise, and adversarial attacks. Researchers used many strategies like data augmentation [59, 60] for better adaptability through attention mechanisms [57], regularization [18, 19], and network architecture design [25]. Among these strategies, diffusion models have emerged as a promising approach due to their ability to denoise data during the adversarial

purification process [5, 29, 32], thereby minimizing the negative impact of data errors on downstream tasks. However, diffusion models have inherent limitations when it comes to robustness. For instance, they struggle to handle erroneous inputs during the inference phase in image generation tasks. It highlights the need for further research and optimization to enhance their robustness. Therefore, researchers are actively exploring various techniques and approaches to enhance the robustness of deep learning models, aiming to improve their resistance against different challenges and ensure reliable performance in real-world applications.

PID control theory. The Proportional Integral Derivative (PID) control theory is a cornerstone concept in automatic control, which achieves effective control of a system through the combination of proportional, integral, and derivative parameters. This theory has been extensively utilized across traditional domains, including industrial process control [30], robotics and automation [8], and aerospace [16], while also undergoing continuous evolution and expansion in tandem with technological advancements. For instance, adaptive PID control [15] can automatically adjust parameters based on changes in system performance, while fuzzy PID control [17] and neural network PID control optimize control [53] performance by incorporating fuzzy logic and neural network technologies. Furthermore, intelligent PID control enhances the adaptability and robustness of the controller by integrating technologies such as machine learning. Despite facing challenges such as model uncertainty, multivariable control, and networked control, research, and applications of PID control theory continue to develop, demonstrating strong vitality and broad prospects.

3 Method

3.1 Problem Analysis

The trained neural network in the forward process enters into the reverse process with the following inference process.

$$x_{t-1} = \frac{1}{\sqrt{\alpha_t}} \left[x_t - \frac{1 - \alpha_t}{\sqrt{1 - \alpha_t}} \left((1 + w)\varepsilon_\theta(x_t, y, t) - w\varepsilon_\theta(x_t, t) \right) \right] + \sigma_t z \quad (1)$$

The mathematical mechanism underlying the reverse sampling process in CDMs involves a trained conditional neural network and an unconditional neural network, denoted as $\varepsilon_\theta(x_t, y, t)$ and $\varepsilon_\theta(x_t, t)$, respectively. The parameter w is manually set to regulate the weighting between the two networks, thus balancing the diversity and relevance of the generated outcomes.

However, when the two well-trained neural networks encounter inaccurate input data during the sampling phase, it can result in a fixed error in the neural network’s output. The concern arises regarding whether this error Δ , accumulating over steps T , could potentially lead to uncontrollable effects in the final generation of the diffusion model.

Theorem 3.1. *Let $\beta_T = \sqrt{1 - \alpha_T}$ and $\bar{\beta}_T = \sqrt{1 - \bar{\alpha}_T}$. Due to the inaccuracy of the input data, the error Δ generated by the neural network during the sampling process can accumulate more than $-\frac{1 - \alpha_T}{\sqrt{\bar{\alpha}_T(1 - \bar{\alpha}_T)}} \Delta$ after T steps of iterations, which leads to uncontrolled model performance.*

Proof. We utilize mathematical induction to examine the accumulation of the final error Δ . The detail proof is provided in Appendix A.3.1. \square

Based on the aforementioned theorem, we have determined that noise from inaccurate inputs is gradually amplified through reverse sampling, adversely affecting the results of the conditional diffusion model. Our objective is to mitigate the amplification and propagation of fixed errors during the sampling process, thereby enhancing the robustness of the conditional diffusion model.

3.2 Robust Conditional Diffusion Model Framework

Our proposed model, RCDM, enhances the performance through a continuous two-stage strategy optimization, which integrates the sequential execution of forward and reverse processes. Initially, the model undergoes iterative training through the forward process, accumulating progressively deepened

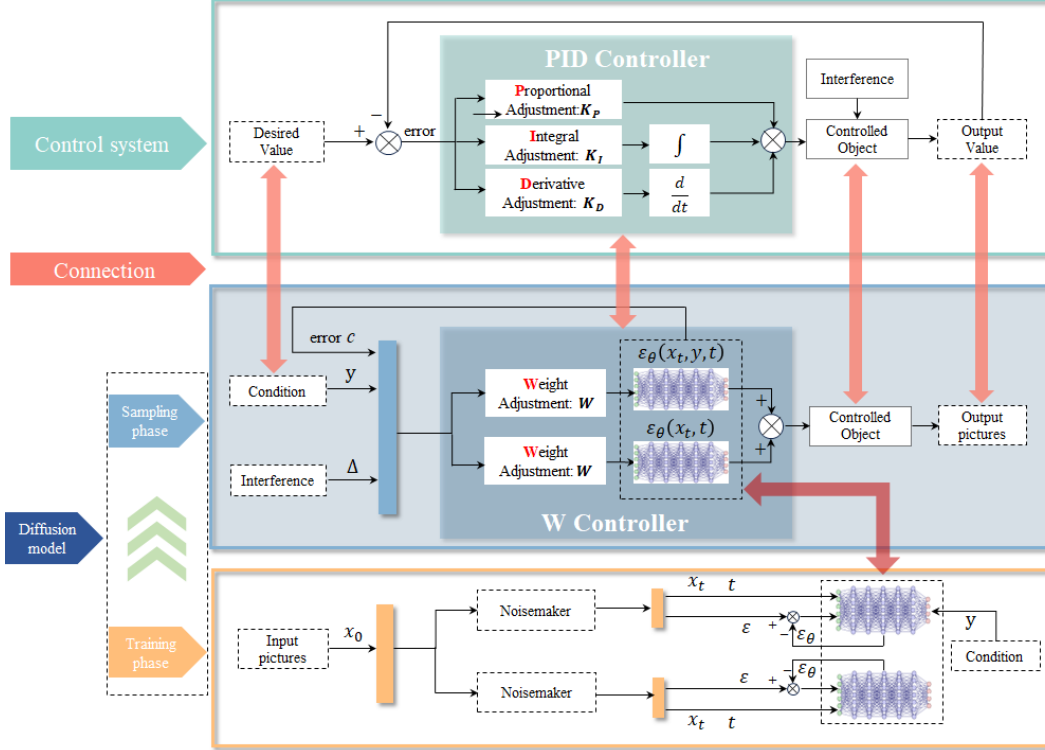


Figure 2: Robust conditional diffusion modeling framework.

learning experiences. Subsequently, upon reaching a preset threshold of iterations, it transitions seamlessly to the reverse process for sampling generation, as detailed in Figure 2.

In the forward phase of a diffusion model, the input image x_0 undergoes progressive noise addition to generate a collection $\{x_t, t, \epsilon\}$, $\{x_t, t, \epsilon, y\}$ that trains both unconditional $\epsilon_\theta(x_t, t)$ and conditional $\epsilon_\theta(x_t, y, t)$ neural networks. After sufficient training, the process shifts from the forward phase to the reverse phase, which is also known as the sampling phase. However, inaccuracies in the input data can lead to fixed errors Δ in the neural network, which can affect the final generation of the image. Therefore, RCDM enhances the ability to resist disturbances by adjusting the parameters w of the two network weights, drawing on the PID control method from control theory. Ultimately, the image is output through the joint iterative action of the Gaussian distribution z and the control signal $[(1 + w)\epsilon_\theta(x_t, y, t) - w\epsilon_\theta(x_t, t)]$.

In the architecture of a robust conditional diffusion model, the design of the filter is one of the key innovations for enhancing the model's robustness. The role of the filter is to optimize the data reconstruction quality in the reverse process by mitigating the impact of errors. In this paper, we concentrate on the derivation of the optimal filter parameters w through a rigorous theoretical framework and associated proof. The objective is to mitigate the effects of input errors inherent in the reverse process, thereby improving the robustness of the data reconstruction.

3.3 Mathematical Modeling

In this part, we will utilize mathematics to characterize the distributional properties of neural networks fitted during the forward process of diffusion models. This study seeks to clarify the discrepancies arising in the outputs of the trained network when erroneous input data are introduced during the generative phase. Furthermore, it aims to investigate the impact of these discrepancies on the model's overall performance and ability to generalize. Then, we will mainly study the extent to which specific parameters decline the perturbations caused by input errors during the generation, to gain a profound understanding of the behavioral mechanisms of neural networks in the presence of input data discrepancies and their subsequent impact on model outputs.

Definition 3.1. Assume that ε_1 and ε_2 represent the truths, that is, the Gaussian noise added at a step during the forward process, such that $\varepsilon_1 \sim (0, I)$ and $\varepsilon_2 \sim (0, I)$. Here, Δ_1 and Δ_2 denote the discrepancies, which are the errors generated by the neural network architecture during the learning process. And the inaccuracy of the input data in the sampling phase causes the neural network to produce a fixed error Δ .

Theorem 3.2. The control signal $[(1+w)\varepsilon_\theta(x_t, y, t) - w\varepsilon_\theta(x_t, t)]$ conforms to distribution $O \sim [(1+w)\Delta_1 - w\Delta_2, ((1+w)^2 + w^2)I]$, $O_L \sim [0, ((1+w)^2 + w^2)I]$ in the ideal case, and $O_G \sim [(1+w)\Delta_1 - w\Delta_2 + \Delta, ((1+w)^2 + w^2)I]$ in the presence of interference.

Proof. The training functions of the two networks $(\varepsilon_\theta(x_t, t), \varepsilon_\theta(x_t, y, t))$ obtained from the forward process training are:

$$\mathbb{E}_{x_0, y \sim \bar{p}(x_0, y), \varepsilon \sim \mathcal{N}(0, I)} \left[\left\| \varepsilon - \varepsilon_\theta(\bar{\alpha}_t x_0 + \bar{\beta}_t \varepsilon, y, t) \right\|^2 \right] \quad (2)$$

$$\mathbb{E}_{x_0 \sim \bar{p}(x_0), \varepsilon \sim \mathcal{N}(0, I)} \left[\left\| \varepsilon - \varepsilon_\theta(\bar{\alpha}_t x_0 + \bar{\beta}_t \varepsilon, t) \right\|^2 \right] \quad (3)$$

$\varepsilon_\theta(x_t, y, t) = \varepsilon_1 + \Delta_1$, $\varepsilon_\theta(x_t, t) = \varepsilon_2 + \Delta_2$. It is evident that ε_1 is the Gaussian noise added at a step of the forward process under the condition y , and ε_2 is the Gaussian noise added under the absence of condition y . These two distributions are independent and uncorrelated. Note that, $O = (1+w)(\varepsilon_1 + \Delta_1) - w(\varepsilon_2 + \Delta_2)$. Then, the form of its distribution can be depicted as Equation 4.

$$O \sim [(1+w)\Delta_1 - w\Delta_2, ((1+w)^2 + w^2)I] \quad (4)$$

In the ideal situation, a well-trained neural network would not produce errors $\Delta_1 = 0$, $\Delta_2 = 0$, $\Delta = 0$, then the expected output distribution is O_L . However, various sources of error may arise in the neural network in the sampling phase, i.e., the trained neural network itself has an error c , and the inaccuracy of the input data in the sampling phase causes the neural network to produce a fixed error Δ , noting that the distribution is O_G . \square

Subsequently, we focus on how the variation in the parameter w affects the generation outcome, then focus on the discrepancy between O_L and O_G at each step. This analysis can assist us in evaluating the performance of the neural network model and in adjusting the parameter w to minimize the error within the generation outcome. Then, we use the intersection area $J(w)$ between the distributions O_L and O_G as a more intuitive and illustrative measure of their similarity compared to the Kullback-Leibler (KL) divergence.

Lemma 3.1. Let $d(w) = (1+w)\Delta_1 - w\Delta_2 + \Delta = 2x_a$, where the sign of $d(w)$ is consistent with the sign of x_a . By applying the method for solving the integral probability density function of the Gaussian distribution, we derive the solution for the half intersection area $I(w)$ between the distributions O_L and O_G as follows.

$$I(w) = \frac{1}{2}J(w) = \frac{1}{2}e^{-\frac{d^2(w)}{8\sigma^2(w)}} \quad (5)$$

The proof of the following properties of $I(w)$ is provided in Appendix A.3.2.

Function $I(w)$ quantifies the degree of overlap between the expected output distribution O_L and the actual generated distribution O_G , an intuitive and concrete representation of their similarity, as depicted in Figure 3. An increase in the parameter w within a certain range enhances function $I(w)$, indicating that the parameter w can improve the model's robustness to disturbances by aligning the actual generated distribution more closely with the ideal distribution, even in the presence of interference. As depicted in Figure 3, x_a represents the x -coordinate of the intersection between distributions O_L and O_G . It is determined by solving the probability density functions of the Gaussian distributions, yielding $x_a = \bar{x}_a = \frac{(1+w)\Delta_1 - w\Delta_2 + \Delta}{2}$.

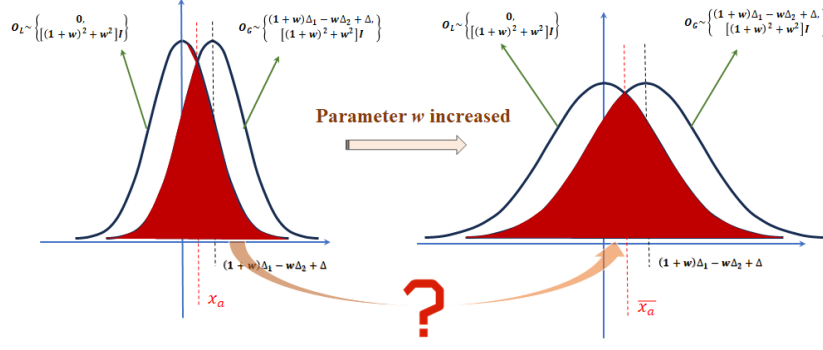


Figure 3: Discrepancy schematic distribution O_L vs. O_G .

3.3.1 Monotonic Constraint

Subsequently, we will explore the range of values for the w for which the function $I(w)$ is monotonically increasing. Therefore, it will increase the intersection area between O_L and O_G , then better align with the ideal scenario and enhance the ability to suppress interference as w increases.

Lemma 3.2. Let $\sigma(w) = [(1+w)^2 + w^2]^{\frac{1}{2}}$ be the standard deviation and $d(w) = (1+w)\Delta_1 - w\Delta_2 + \Delta$. Assume that the monotonic of the function $I(w)$ is independent of $\sigma(w)$, then the function $I(w)$ is monotonically increasing within the range $\left[0, \frac{|\Delta|}{2c} - \frac{1}{2}\right]$.

Proof. This proof aims to analyze the monotonic of the function $I(w)$ concerning the parameter w . The specific analysis process is as follows.

- (1) Firstly, based on different values of x_a and $2\Delta + \Delta_1 + \Delta_2$, the monotonic increasing intervals of the function $I(w)$ are determined.
- (2) In these monotonically increasing intervals, only some cases satisfy the prerequisite condition $w > 0$. Therefore, it is necessary to ensure that regardless of the variations in Δ , Δ_1 and Δ_2 , both the values of x_a and $2\Delta + \Delta_1 + \Delta_2$ remain within these feasible ranges.

The detail proof is provided in Appendix A.3.3. □

3.3.2 Function Value Constraint

Within the intersection region $J(w)$ between distributions O_L and O_G , the function is increasing within the range $\left[0, \frac{|\Delta|}{2c} - \frac{1}{2}\right]$. However, beyond the value of $\frac{|\Delta|}{2c} - \frac{1}{2}$, the function may also continue to increase monotonically with a certain probability. Therefore, $J\left(\frac{|\Delta|}{2c} - \frac{1}{2}\right)$ is not necessarily the maximum value. Furthermore, whether $J\left(\frac{|\Delta|}{2c} - \frac{1}{2}\right)$ satisfies the value function constraint $J(w) = 1$ is a question that warrants in-depth consideration. If $J\left(\frac{|\Delta|}{2c} - \frac{1}{2}\right)$ does not satisfy the value function constraint $J(w) = 1$, then adjusting the parameter w to meet this constraint may conflict with the monotonic constraint of the function being monotonically increasing over the interval $\left[0, \frac{|\Delta|}{2c} - \frac{1}{2}\right]$.

Lemma 3.3. Let the constant n as the balancing factor, determined experimentally. When $w = \frac{n|\Delta|}{2c} - \frac{1}{2}$, both monotonic and value constraints are generally satisfied, achieving equilibrium.

Proof. In analyzing the interrelationship between the monotonic constraint and the value constraint $J(w) = 1$, the variable $d(w)$ plays an essential role. Taking $2\Delta + \Delta_1 + \Delta_2 > 0$ as an example, to ensure the monotonic increase of the function $J(w)$ for $w > 0$, $d(w)$ must remain non-negative. However, to satisfy the value constraint $J(w) = 1$, $d(w)$ must be constantly zero. Although $d(w) = 0$ can simultaneously satisfy these two conditions, due to Δ_1 and Δ_2 being random variables, $d(w)$ itself possesses randomness and cannot be guaranteed to remain constant. Therefore, by analyzing the probability density function of $d(w)$ when $w = \frac{n|\Delta|}{2c} - \frac{1}{2}$, we can observe how the balancing

factor n cleverly resolves the conflicts between these constraints. The detail proof is provided in Appendix A.3.4. \square

4 Experiments and Discussion

For the experiments detailed below, we employed two NVIDIA V100 GPUs with 32 gigabytes (GB) of memory each. To enhance reproducibility, we present our robust diffusion model framework through pseudocode. This standardized abstraction simplifies intricate operations, aiding comprehension and replication within the research community. The algorithmic workflow covers iterative training in the forward process of neural networks, as well as the design of filters and controllers in the reverse process. Please refer to Algorithms 1~2 for details in Appendix A.2.

4.1 Validation on MNIST Dataset

Exploring the determinacy of the balancing factor n in the theory presents a challenge due to its elusive theoretical derivation. Our study adopts a semi-theoretical, semi-empirical approach, leveraging MNIST dataset to analyze the plausible range of n values. The choice of MNIST dataset is twofold. Firstly, its relative simplicity allows us to focus on the impact of the balancing factor n . Secondly, conducting experiments under various systematic error conditions enhances the generalizability of the discovered balancing factor n and provides a comprehensive assessment of its applicability.

To validate the generalizability of the balance factor n , we tested the performance of different parameter w values under four distinct fixed errors Δ (0.3, -0.3, +3, -3). Through these experiments, we aimed to explore whether the range of values for the balance factor n remains consistent across different error levels, thereby indirectly verifying the rationality of our approach. The experimental results are presented in Figures 4~5, providing preliminary insights into the range of values for the balance factor n . Additional generation results are shown in Appendix A.4.1

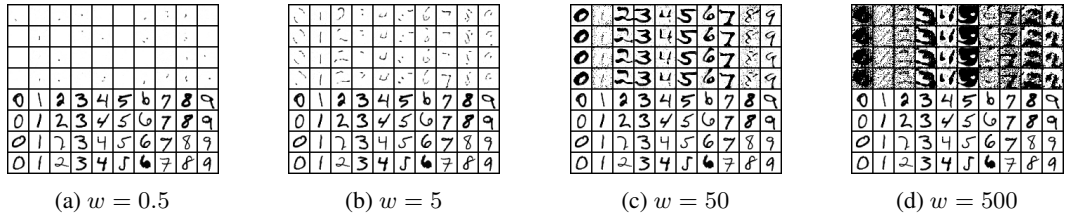


Figure 4: Reflections of $\Delta = 0.3$ on different parameters w . With $w = 50$, the model can generate numbers in the presence of errors.

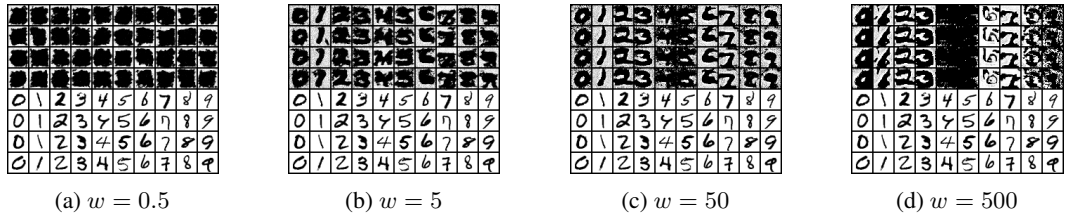


Figure 5: Reflections of $\Delta = -0.3$ on different parameters w . With $w = 50$, the model can generate numbers in the presence of errors.

In experiments on MNIST dataset, we studied how fixed error Δ affect parameter w selection. We found that optimal model performance requires adjusting w for different error levels. For fixed error $\Delta = \pm 0.3$, $w = 50$ was optimal, while $\Delta = 3$ required $w = 5000$. Analysis revealed lower image quality at $\Delta = -3$ compared to $+3$, possibly due to pixel normalization constraints, suggesting a model robustness threshold. Despite these variations, an optimal n of around 185 was inferred from comparisons across error conditions. To maintain model robustness and image quality, we suggest adjusting w based on error magnitude while keeping n near 185. This strategy ensures adaptability to diverse error scenarios, supporting high-quality image generation for various applications.

4.2 Validation on CIFAR-10 Dataset

To ascertain the suitability of $n=185$ beyond MNIST dataset, we extended our experiments to the more complex CIFAR-10 dataset. The increased complexity of CIFAR-10 offers a stringent test for our model. We employed the Fréchet Inception Distance (FID) to mitigate the subjectivity inherent in visual assessment. FID evaluates the statistical similarity between the feature representations of generated and actual images, with a lower score indicating a closer distribution match and superior image generation quality. Furthermore, we modified the neural network architecture and sampling mode alongside the dataset to comprehensively test the robustness of the balance factor n . This approach ensures that our conclusions are not confined to a specific neural network and sampling mode configuration, enhancing the generalizability of our findings.

The FID assessments across varied neural network architectures on CIFAR-10 dataset reinforce and expand upon the conclusions drawn from MNIST. This cross-architecture and cross-dataset validation strengthens the scientific rigor of our research and offers a more profound understanding of the model’s performance across different conditions.

Table 1: Generated outcomes of Δ on w across network structures and sampling modes. The optimal w is set between the two bolded w .

Sampling mode	Δ	w	Network structure	
			U-net	U-vit
DDIM	0	0	3.572	4.109
		5	96.745	97.630
		10	42.278	48.867
		20	37.934	41.627
		20	43.512	37.980
DDPM	0.03	0	543.202	609.914
		50	90.171	77.047
		100	105.414	87.249
		0	62.066	66.079
		5	38.828	37.902
DDIM	-0.03	10	41.387	35.453
		20	46.459	35.720
		0	416.859	424.844
		50	83.808	66.923
		100	90.447	69.050

In this study, we systematically investigated the impact of w on the generative outcomes under various fixed error Δ through a series of controlled experiments. The findings indicated a notable decrease in the influence of errors on the final generation results within a particular range of increasing w , as evidenced by the decline in the FID score. Specifically, as w increased, the FID score generally showed a downward trend, indicating a reduction in the distributional difference between the generated and authentic images, thereby validating our hypothesis regarding the impact of w adjustment on generation quality. Furthermore, we examined the changes in the FID index under different network structures and sampling modes, further revealing the adaptability and effectiveness of w adjustment under various conditions. Experiments conducted on MNIST dataset indicated that setting the balance factor to 185 could significantly enhance the robustness of the diffusion model. Cross-validation revealed that the parameter w setting corresponding to this balancing factor could notably improve the model’s resistance to error on CIFAR-10 dataset.

However, when we further increased w , for instance, by adjusting the balance factor to 120, we observed a slight enhancement in the model’s anti-interference capability. This phenomenon differs from the experimental results of MNIST dataset, which we attribute primarily to MNIST dataset’s w being determined based on perceptual judgment and the sparse parameter settings in the experiments. Notably, in the experiments on CIFAR-10 dataset, when the neural network structure was U-vit and the sampling method was DDIM, the result with w set to 20 outperformed that with w set to 185,

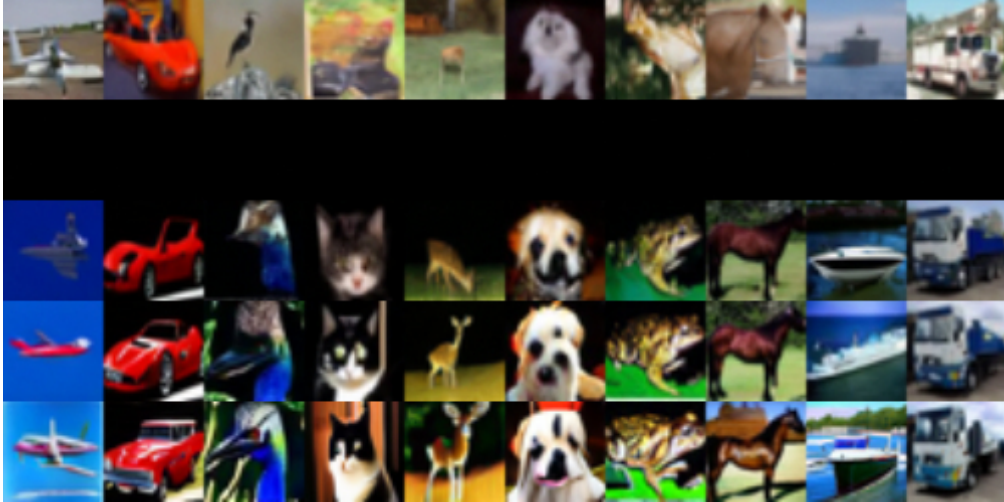


Figure 6: Visualization of the final generation results in $\Delta = 0.03$, DDPM and U-net on CIFAR-10 dataset. The top row of the image illustrates the ideal state where the CDM generates images without any error. Subsequent 2~5 rows, demonstrate the images produced by RCDM with the w set to **0, 5, 10, and 20**, respectively.

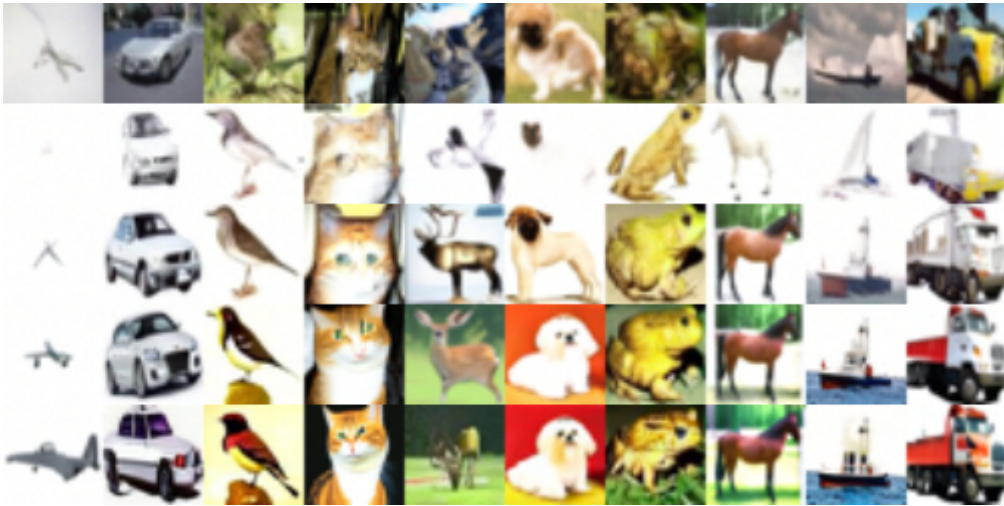


Figure 7: Visualization of the final generation results in $\Delta = -0.03$, DDIM and U-vit on CIFAR-10 dataset. The top row of the image illustrates the ideal state where CDM generates images without any error. Subsequent 2~5 rows, demonstrate the images produced by RCDM with the w set to **0, 5, 10, and 20**, respectively.

contrasting with other experimental outcomes. We speculate that this occurrence may stem from two reasons: firstly, the formula for setting the optimal w is a semi-empirical formula that combines theoretical analysis with practical experience and may have certain inaccuracies. Secondly, the range of optimal w determined experimentally is relatively limited.

Our findings suggest that setting the balance factor to 185 can provide sufficient robustness for the diffusion model in most cases. Pursuing a larger balance factor may result in only a slight improvement in robustness, which may not be cost-effective. In addition, the comparison between experimental results with and without error input demonstrates that although w can enhance the model’s robustness and mitigate the impact of errors to some extent, it cannot eliminate errors. Therefore, reducing error input remains critical for improving the quality of generation outcomes.

These discoveries not only provide a solid theoretical foundation for parameter adjustment in generative models but also, have significant practical guidance for error control and quality optimization.

Through these experiments, we have provided a systematic methodology for parameter optimization in generative models, which will guide future research and application development.

5 Conclusion

This study presents the Robust Conditional Diffusion Model (RCDM), which enhances the robustness of diffusion models by considering collaborative interaction between two neural networks based on control theory. RCDM optimizes the weighting of two neural networks during sampling without additional computational costs, maintaining efficiency and adaptability. Experimental results on MNIST and CIFAR-10 datasets demonstrate significant improvements in robustness without compromising inference speed, making it practical for real-time applications. Our proposed model is a trade-off strategy that reduces the diversity of model outputs to some extent but still achieves acceptable results in extreme cases. Overall, this work strengthens diffusion model robustness, advancing neural network-based machine learning systems and enabling more reliable AI solutions.

References

- [1] Fan Bao, Shen Nie, Kaiwen Xue, Yue Cao, Chongxuan Li, Hang Su, and Jun Zhu. All are worth words: A vit backbone for diffusion models. In *Proceedings of the IEEE/CVF Conference on Computer Vision and Pattern Recognition*, pages 22669–22679, 2023.
- [2] Kevin Black, Michael Janner, Yilun Du, Ilya Kostrikov, and Sergey Levine. Training diffusion models with reinforcement learning. *arXiv preprint arXiv:2305.13301*, 2023.
- [3] Tsachi Blau, Roy Ganz, Bahjat Kawar, Alex Bronstein, and Michael Elad. Threat model-agnostic adversarial defense using diffusion models. *arXiv preprint arXiv:2207.08089*, 2022.
- [4] Valentin De Bortoli, Emile Mathieu, MJ Hutchinson, James Thornton, Yee Whye Teh, and Arnaud Doucet. Riemannian score-based generative modelling. *Advances in Neural Information Processing Systems*, page 46, 2022.
- [5] Nicholas Carlini, Florian Tramer, Krishnamurthy Dj Dvijotham, Leslie Rice, Mingjie Sun, and J Zico Kolter. (certified!!) adversarial robustness for free! *arXiv preprint arXiv:2206.10550*, 2022.
- [6] Minshuo Chen, Song Mei, Jianqing Fan, and Mengdi Wang. An overview of diffusion models: Applications, guided generation, statistical rates and optimization. *arXiv preprint arXiv:2404.07771*, 2024.
- [7] Xiwei Cheng, Kexin Fu, and Farzan Farnia. Stability and Generalization in Free Adversarial Training. *arXiv e-prints*, page arXiv:2404.08980, April 2024.
- [8] Phichitphon Chotikunann, Rawiphon Chotikunann, Anuchit Nirapai, Anantasak Wongkamhang, Pariwat Imura, and Manas Sangworasil. Optimizing membership function tuning for fuzzy control of robotic manipulators using pid-driven data techniques. *Journal of Robotics and Control (JRC)*, 4(2):128–140, 2023.
- [9] Li chu, Xiao bingjia, and Yuan qiping. UnetTSF: A Better Performance Linear Complexity Time Series Prediction Model. *arXiv e-prints*, page arXiv:2401.03001, January 2024.
- [10] Erick Delage and Yinyu Ye. Distributionally robust optimization under moment uncertainty with application to data-driven problems. *Operations research*, 58(3):595–612, 2010.
- [11] Prafulla Dhariwal and Alexander Nichol. Diffusion models beat gans on image synthesis. *Advances in neural information processing systems*, 34:8780–8794, 2021.
- [12] Tim Dockhorn, Arash Vahdat, and Karsten Kreis. Score-based generative modeling with critically-damped langevin diffusion. In *International Conference on Learning Representations*, 2021.
- [13] Hengyu Fu, Zhuoran Yang, Mengdi Wang, and Minshuo Chen. Unveil conditional diffusion models with classifier-free guidance: A sharp statistical theory. *arXiv preprint arXiv:2403.11968*, 2024.
- [14] Shanghua Gao, Pan Zhou, Ming-Ming Cheng, and Shuicheng Yan. Masked diffusion transformer is a strong image synthesizer. In *Proceedings of the IEEE/CVF International Conference on Computer Vision*, pages 23164–23173, 2023.

- [15] Seyyed Morteza Ghamari, Fatemeh Khavari, and Hasan Mollaei. Lyapunov-based adaptive pid controller design for buck converter. *Soft Computing*, 27(9):5741–5750, 2023.
- [16] Ayhan Gün. Attitude control of a quadrotor using pid controller based on differential evolution algorithm. *Expert Systems with Applications*, 229:120518, 2023.
- [17] Jiale Han, Xianlei Shan, Haitao Liu, Juliang Xiao, and Tian Huang. Fuzzy gain scheduling pid control of a hybrid robot based on dynamic characteristics. *Mechanism and Machine Theory*, 184:105283, 2023.
- [18] Zongbo Han, Yifeng Yang, Changqing Zhang, Linjun Zhang, Joey Tianyi Zhou, Qinghua Hu, and Huaxiu Yao. Selective learning: Towards robust calibration with dynamic regularization. *arXiv preprint arXiv:2402.08384*, 2024.
- [19] Degan Hao, Dooman Arefan, Margarita Zuley, Wendie Berg, and Shandong Wu. Adversarially robust feature learning for breast cancer diagnosis. *arXiv preprint arXiv:2402.08768*, 2024.
- [20] Jonathan Ho, Ajay Jain, and Pieter Abbeel. Denoising diffusion probabilistic models. *Advances in neural information processing systems*, 33:6840–6851, 2020.
- [21] Jonathan Ho, Chitwan Saharia, William Chan, David J Fleet, Mohammad Norouzi, and Tim Salimans. Cascaded diffusion models for high fidelity image generation. *Journal of Machine Learning Research*, 23(47):1–33, 2022.
- [22] Jonathan Ho and Tim Salimans. Classifier-free diffusion guidance. *arXiv preprint arXiv:2207.12598*, 2022.
- [23] Chin-Wei Huang, Jae Hyun Lim, and Aaron C Courville. A variational perspective on diffusion-based generative models and score matching. *Advances in Neural Information Processing Systems*, 34:22863–22876, 2021.
- [24] Jaehyeong Jo, Seul Lee, and Sung Ju Hwang. Score-based generative modeling of graphs via the system of stochastic differential equations. In *International Conference on Machine Learning*, pages 10362–10383. PMLR, 2022.
- [25] William Kengne and Modou Wade. Robust deep learning from weakly dependent data. *arXiv preprint arXiv:2405.05081*, 2024.
- [26] Daniel Kuhn, Peyman Mohajerin Esfahani, Viet Anh Nguyen, and Soroosh Shafieezadeh-Abadeh. Wasserstein distributionally robust optimization: Theory and applications in machine learning. In *Operations research & management science in the age of analytics*, pages 130–166. INFORMS, 2019.
- [27] MUYANG LI, Tianle Cai, Jiaxin Cao, Qinsheng Zhang, Han Cai, Junjie Bai, Yangqing Jia, Ming-Yu Liu, Kai Li, and Song Han. DistriFusion: Distributed Parallel Inference for High-Resolution Diffusion Models. *arXiv e-prints*, page arXiv:2402.19481, February 2024.
- [28] Fengming Lin, Xiaolei Fang, and Zheming Gao. Distributionally robust optimization: A review on theory and applications. *Numerical Algebra, Control and Optimization*, 12(1):159–212, 2022.
- [29] Guang Lin, Zerui Tao, Jianhai Zhang, Toshihisa Tanaka, and Qibin Zhao. Robust diffusion models for adversarial purification. *arXiv preprint arXiv:2403.16067*, 2024.
- [30] Lu Liu, Dingyu Xue, and Shuo Zhang. General type industrial temperature system control based on fuzzy fractional-order pid controller. *Complex & Intelligent Systems*, 9(3):2585–2597, 2023.
- [31] Xihui Liu, Dong Huk Park, Samaneh Azadi, Gong Zhang, Arman Chopikyan, Yuxiao Hu, Humphrey Shi, Anna Rohrbach, and Trevor Darrell. More control for free! image synthesis with semantic diffusion guidance. In *Proceedings of the IEEE/CVF Winter Conference on Applications of Computer Vision*, pages 289–299, 2023.
- [32] Yiming Liu, Kezhao Liu, Yao Xiao, Ziyi Dong, Xiaogang Xu, Pengxu Wei, and Liang Lin. Towards Better Adversarial Purification via Adversarial Denoising Diffusion Training. *arXiv e-prints*, page arXiv:2404.14309, April 2024.
- [33] Cheng Lu, Kaiwen Zheng, Fan Bao, Jianfei Chen, Chongxuan Li, and Jun Zhu. Maximum likelihood training for score-based diffusion odes by high order denoising score matching. In *International Conference on Machine Learning*, pages 14429–14460. PMLR, 2022.

- [34] Alexander Quinn Nichol and Prafulla Dhariwal. Improved denoising diffusion probabilistic models. In *International conference on machine learning*, pages 8162–8171. PMLR, 2021.
- [35] Axi Niu, Trung X Pham, Kang Zhang, Jinqiu Sun, Yu Zhu, Qingsen Yan, In So Kweon, and Yanning Zhang. Acdmsr: Accelerated conditional diffusion models for single image super-resolution. *IEEE Transactions on Broadcasting*, 2024.
- [36] William Peebles and Saining Xie. Scalable diffusion models with transformers. In *Proceedings of the IEEE/CVF International Conference on Computer Vision*, pages 4195–4205, 2023.
- [37] Stanislav Pidhorskyi, Donald A. Adjeroh, and Gianfranco Doretto. Adversarial latent autoencoders. In *2020 IEEE/CVF Conference on Computer Vision and Pattern Recognition (CVPR)*, pages 14092–14101, 2020.
- [38] Kashif Rasul, Calvin Seward, Ingmar Schuster, and Roland Vollgraf. Autoregressive denoising diffusion models for multivariate probabilistic time series forecasting. In *International Conference on Machine Learning*, pages 8857–8868. PMLR, 2021.
- [39] Tim Salimans and Jonathan Ho. Progressive distillation for fast sampling of diffusion models. In *International Conference on Learning Representations*, 2022.
- [40] Saurabh Saxena, Charles Herrmann, Junhwa Hur, Abhishek Kar, Mohammad Norouzi, Deqing Sun, and David J Fleet. The surprising effectiveness of diffusion models for optical flow and monocular depth estimation. *Advances in Neural Information Processing Systems*, 36, 2024.
- [41] Chence Shi, Shitong Luo, Minkai Xu, and Jian Tang. Learning gradient fields for molecular conformation generation. In *International conference on machine learning*, pages 9558–9568. PMLR, 2021.
- [42] Jascha Sohl-Dickstein, Eric Weiss, Niru Maheswaranathan, and Surya Ganguli. Deep unsupervised learning using nonequilibrium thermodynamics. In *International conference on machine learning*, pages 2256–2265. PMLR, 2015.
- [43] Yang Song and Stefano Ermon. Improved techniques for training score-based generative models. *Advances in neural information processing systems*, 33:12438–12448, 2020.
- [44] Yang Song, Jascha Sohl-Dickstein, Diederik P Kingma, Abhishek Kumar, Stefano Ermon, and Ben Poole. Score-based generative modeling through stochastic differential equations. *arXiv preprint arXiv:2011.13456*, 2020.
- [45] Hado Van Hasselt, Arthur Guez, and David Silver. Deep reinforcement learning with double q-learning. In *Proceedings of the AAAI conference on artificial intelligence*, volume 30, 2016.
- [46] Jinyi Wang, Zhaoyang Lyu, Dahua Lin, Bo Dai, and Hongfei Fu. Guided diffusion model for adversarial purification. *arXiv preprint arXiv:2205.14969*, 2022.
- [47] Le Wang, Ruiyun Qi, and Bin Jiang. Adaptive fault-tolerant optimal control for hypersonic vehicles with state constraints based on adaptive dynamic programming. *Journal of the Franklin Institute*, page 106833, 2024.
- [48] Yongkang Wang, Xuan Liu, Feng Huang, Zhankun Xiong, and Wen Zhang. A multi-modal contrastive diffusion model for therapeutic peptide generation. In *Proceedings of the AAAI Conference on Artificial Intelligence*, volume 38, pages 3–11, 2024.
- [49] Quanlin Wu, Hang Ye, and Yuntian Gu. Guided diffusion model for adversarial purification from random noise. *arXiv preprint arXiv:2206.10875*, 2022.
- [50] Xuanting Xie, Zhao Kang, and Wenyu Chen. Robust graph structure learning under heterophily. *arXiv preprint arXiv:2403.03659*, 2024.
- [51] Can Xu, Haosen Wang, Weigang Wang, Pengfei Zheng, and Hongyang Chen. Geometric-facilitated denoising diffusion model for 3d molecule generation. *arXiv preprint arXiv:2401.02683*, 2024.
- [52] Minkai Xu, Lantao Yu, Yang Song, Chence Shi, Stefano Ermon, and Jian Tang. Geodiff: A geometric diffusion model for molecular conformation generation. *arXiv preprint arXiv:2203.02923*, 2022.
- [53] Ahmed H Yakout, Masoud Dashtdar, Kareem M AboRas, Yazeed Yasin Ghadi, Ahmed Elzawawy, Amr Yousef, and Hossam Kotb. Neural network-based adaptive pid controller design for over-frequency control in microgrid using honey badger algorithm. *IEEE Access*, 12:27989–28005, 2024.

- [54] Ruihan Yang and Stephan Mandt. Lossy image compression with conditional diffusion models. *Advances in Neural Information Processing Systems*, 36, 2024.
- [55] Yichen Yang, Xin Liu, and Kun He. Fast Adversarial Training against Textual Adversarial Attacks. *arXiv e-prints*, page arXiv:2401.12461, January 2024.
- [56] Jongmin Yoon, Sung Ju Hwang, and Juho Lee. Adversarial purification with score-based generative models. In *International Conference on Machine Learning*, pages 12062–12072. PMLR, 2021.
- [57] Han Zhang, Medhat Elsayed, Majid Bavand, Raimundas Gaigalas, Yigit Ozcan, and Melike Erol-Kantarci. Federated learning with dual attention for robust modulation classification under attacks. *arXiv preprint arXiv:2401.11039*, 2024.
- [58] Lvmin Zhang, Anyi Rao, and Maneesh Agrawala. Adding conditional control to text-to-image diffusion models. In *Proceedings of the IEEE/CVF International Conference on Computer Vision*, pages 3836–3847, 2023.
- [59] Yuhang Zheng, Zhen Wang, and Long Chen. Improving data augmentation for robust visual question answering with effective curriculum learning. *arXiv preprint arXiv:2401.15646*, 2024.
- [60] Zhenyu Zhou, Junhui Chen, Namin Wang, Lantian Li, and Dong Wang. Adversarial data augmentation for robust speaker verification. In *Proceedings of the 2023 9th International Conference on Communication and Information Processing*, pages 226–230, 2023.

A Appendix

A.1 Conditional Diffusion Model

Conditional diffusion models are identical to diffusion models in that they have two processes, i.g. forward process and reverse process. The mathematical mechanism of conditional diffusion models can be summarized as follows.

Forward Process. During the forward diffusion phase, the model gradually adds Gaussian noise to the data through a series of timesteps t . At each step, the data x_{t-1} is perturbed by Gaussian noise with variance β_t to generate a new latent variable x_t .

$$q(x_t|x_{t-1}) = N(x_t; \sqrt{1 - \beta_t}x_{t-1}, \beta_t\mathbf{I}), \quad (6)$$

Reverse Process. After numerous steps in forward diffusion, the data x_T approaches a Gaussian distribution. The model must learn to recover the original data from the noise through the reverse process, typically achieved by training a neural network to predict the mean $\mu_\theta(\mathbf{x}_t, t)$ and variance $\Sigma_\theta(\mathbf{x}_t, t)$ of each step.

$$p_\theta(\mathbf{x}_{t-1}|\mathbf{x}_t) = \mathcal{N}(\mathbf{x}_{t-1}; \mu_\theta(\mathbf{x}_t, t), \Sigma_\theta(\mathbf{x}_t, t)), \quad (7)$$

Conditional Guidance. Conditional Diffusion Models guide the generation process by incorporating additional conditional information (e.g., class labels or text embeddings). The incorporation of the condition y into each step of the diffusion process is what enables the generation mechanism to be contingent upon this conditioning data.

$$p_\theta(\mathbf{x}_{0:T}|y) = p_\theta(\mathbf{x}_T) \prod_{t=1}^T p_\theta(\mathbf{x}_{t-1}|\mathbf{x}_t, y), \quad (8)$$

Joint Training. In [22], the conditional diffusion model is trained jointly with the unconditional model, allowing the model to learn how to generate both conditional and unconditional samples.

$$\tilde{\varepsilon}_\theta(x_t, y, t) = (1 + w)\varepsilon_\theta(x_t, y, t) - w\varepsilon_\theta(x_t, t), \quad (9)$$

A.2 Experimental Pseudocode

In this section, we provided pseudocode for implementing RCDM to facilitate a more direct comprehension of the algorithm’s logical sequence for the reader. RCDM shares structural similarities with CDM, both comprising a forward and a reverse process. During the forward process, training involves both a non-conditional neural network and a conditional neural network. The core advantage of

RCDM lies in its reverse process, where the weight w of both networks can be dynamically adjusted based on the magnitude of the error, thereby enhancing the model’s robustness. Consequently, RCDM, through the dynamic adjustment of w during the reverse process, strengthens its capability to generate high-quality images in environments with interference.

Algorithm 1 Training phase

- 1: **repeat**
 - 2: $\mathbf{x}_0 \sim q(\mathbf{x}_0)$
 - 3: $t \sim \text{Uniform}(\{1, \dots, T\})$
 - 4: $\varepsilon \sim \mathcal{N}(\mathbf{0}, \mathbf{I})$
 - 5: Stepwise gradient descent
 - Unconditional neural network:
$$\nabla_{\theta} \|\varepsilon - \varepsilon_{\theta}(\sqrt{\bar{\alpha}_t} \mathbf{x}_0 + \sqrt{1 - \bar{\alpha}_t} \varepsilon, t)\|^2$$
 - Conditional neural network
$$\nabla_{\theta} \|\varepsilon - \varepsilon_{\theta}(\sqrt{\bar{\alpha}_t} \mathbf{x}_0 + \sqrt{1 - \bar{\alpha}_t} \varepsilon, y, t)\|^2$$
 - 6: **until** converged
-

Algorithm 2 Sampling phase

- 1: $\mathbf{x}_T \sim \mathcal{N}(\mathbf{0}, \mathbf{I})$
 - 2: **for** $t = T, \dots, 1$ **do**
 - 3: $\mathbf{z} \sim \mathcal{N}(\mathbf{0}, \mathbf{I})$ if $t > 1$, else $\mathbf{z} = \mathbf{0}$
 - 4: Filter math formula
$$w = \frac{n|\Delta|}{2c} - \frac{1}{2}$$
 - 5: Controller signal
$$\tilde{\varepsilon}_{\theta} = [(1 + w)\varepsilon_{\theta}(x_t, y, t) - w\varepsilon_{\theta}(x_t, t)]$$
 - 6: Generator signal
$$\mathbf{x}_{t-1} = \frac{1}{\sqrt{\alpha_t}} \left(\mathbf{x}_t - \frac{1 - \alpha_t}{\sqrt{1 - \bar{\alpha}_t}} \tilde{\varepsilon}_{\theta} \right) + \sigma_t \mathbf{z}$$
 - 7: **end for**
 - 8: **return** \mathbf{x}_0
-

A.3 Proofs

In this section, we provided the proofs for our main theoretical results (Theorem 3.1 and Lemmas 3.1 ~ 3.3).

A.3.1 Proof for Theorem 3.1

We utilized mathematical induction to examine the accumulation of the final error Δ .

$$\begin{aligned}
X_T &: 0 \\
X_{T-1} &: -\frac{\beta_T^2}{\sqrt{\alpha_T}} \frac{\beta_T}{\bar{\beta}_T} \Delta \\
X_{T-2} &: -\left(\frac{\beta_T^2}{\sqrt{\alpha_{T-1} \alpha_T} \beta_T} + \frac{\beta_{T-1}^2}{\sqrt{\alpha_{T-1}} \bar{\beta}_{T-1}} \right) \Delta \\
&\dots\dots \\
X_0 &: -\left(\frac{\beta_T^2}{\sqrt{\alpha_T} \beta_T} + \frac{\beta_{T-1}^2}{\sqrt{\alpha_{T-1}} \bar{\beta}_{T-1}} + \dots + \frac{\beta_1^2}{\sqrt{\alpha_1} \beta_1} \right) \Delta
\end{aligned} \tag{10}$$

Here, $\beta_T = \sqrt{1 - \alpha_T}$, $\bar{\beta}_T = \sqrt{1 - \bar{\alpha}_T}$. We focused on the maximum term $-\frac{\beta_T^2}{\sqrt{\alpha_T} \beta_T} \Delta = -\frac{1 - \alpha_T}{\sqrt{\alpha_T(1 - \bar{\alpha}_T)}} \Delta$. When T is large and $\bar{\alpha}_T$ is very small, any inaccuracies in the input data that result in systematic errors in the neural network’s output will cause the maximum term to become exceedingly large. Thus, the errors arising from the neural network’s response to input inaccuracies will undergo substantial amplification through coefficient multiplication, ultimately leading to a loss of control over the final generation effect.

A.3.2 Proof for Lemma 3.1

Due to the symmetry of the area where O_G intersects O_L , half the size of its area reflects the variation of the intersecting area with the parameter w , as shown in Figure A.1

According to the nature of Gaussian distribution, the expression of this area function as follows.

- (1) $x_a \geq 0$

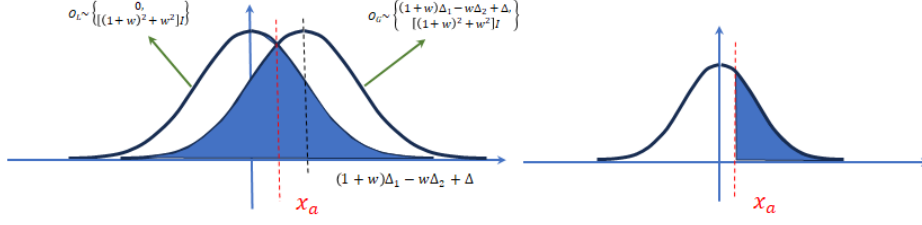


Figure A.1: Description of the area function $J(w)$.

$$I(w) = \int_{\frac{d(w)}{2}}^{+\infty} \frac{1}{\sqrt{2\pi}\sigma(w)} e^{-\frac{x^2}{2\sigma(w)^2}} dx \quad (11)$$

(2) $x_a < 0$

$$I(w) = \int_{-\infty}^{-\frac{d(w)}{2}} \frac{1}{\sqrt{2\pi}\sigma(w)} e^{-\frac{x^2}{2\sigma(w)^2}} dx \quad (12)$$

We referred to the method of solving the integral probability density function of the Gaussian distribution. For $x_a \geq 0$, let $z = \frac{x}{\sigma}$, then $dx = \sigma(w)dz$. Given that $\frac{d}{2} \leq x \leq +\infty$, it follows that $\frac{d}{2\sigma} \leq z \leq +\infty$. We assumed the standard deviation $\sigma > 0$. The case for $\sigma < 0$ yields identical results in the subsequent derivation of the proof, making the discussion of the sign of σ moot. The condition $\sigma \neq 0$ is sufficient for our analysis.

$$I(w) = \int_{\frac{d(w)}{2\sigma(w)}}^{+\infty} \frac{1}{\sqrt{2\pi}} e^{-\frac{z^2}{2}} dz \quad (13)$$

$$I^2(w) = \int_{\frac{d(w)}{2\sigma(w)}}^{+\infty} \frac{1}{\sqrt{2\pi}} e^{-\frac{a^2}{2}} da \int_{\frac{d(w)}{2\sigma(w)}}^{+\infty} \frac{1}{\sqrt{2\pi}} e^{-\frac{b^2}{2}} db = \frac{1}{2\pi} \int_{\frac{d(w)}{2\sigma(w)}}^{+\infty} \int_{\frac{d(w)}{2\sigma(w)}}^{+\infty} e^{-\frac{(a^2+b^2)}{2}} dadb \quad (14)$$

Let $a = r\cos\theta$, $b = r\sin\theta$ in polar coordinates, then $dadb = r dr d\theta$.

$$\begin{aligned} I^2(w) &= \frac{1}{2\pi} \int_0^{\frac{\pi}{2}} d\theta \int_{\frac{\sqrt{2}d(w)}{2\sigma(w)}}^{+\infty} e^{-\frac{r^2}{2}} r dr \\ &= \frac{1}{4} \int_{\frac{\sqrt{2}d(w)}{2\sigma(w)}}^{+\infty} e^{-\frac{r^2}{2}} d\frac{r^2}{2} \\ &= \frac{1}{4} \int_{\frac{d^2(w)}{4\sigma^2(w)}}^{+\infty} e^{-c} dc \\ &= \frac{1}{4} (-e^{-c}) \Big|_{\frac{d^2(w)}{4\sigma^2(w)}}^{+\infty} \\ &= \frac{1}{4} e^{-\frac{d^2(w)}{4\sigma^2(w)}} \end{aligned} \quad (15)$$

When $x_a \geq 0$, the function $I(w) = \frac{1}{2} e^{-\frac{d^2(w)}{8\sigma^2(w)}}$. Similarly, when $x_a < 0$, the function $I(w) = \frac{1}{2} e^{-\frac{d^2(w)}{8\sigma^2(w)}}$. In conclusion, regardless of the value of x_a , the function $I(w) = \frac{1}{2} e^{-\frac{d^2(w)}{8\sigma^2(w)}}$.

A.3.3 Proof for Lemma 3.2

Obviously, the function $J(w)$ agrees with the monotonic of the function $I(w)$ as in Equation 5.

(1) When $x_a > 0$, that is $d(w) > 0$.

$$\begin{aligned}
I'(w) &= \frac{1}{2} e^{-\frac{d^2(w)}{8\sigma^2(w)}} \cdot \left(-\frac{d^2(w)}{8\sigma^2(w)}\right)' \geq 0 \\
&\quad \left(-\frac{d^2(w)}{8\sigma^2(w)}\right)' \geq 0 \\
-\frac{16d'(w)d(w)\sigma^2(w) - 16\sigma'(w)\sigma(w)d^2(w)}{64\sigma^4(w)} &\geq 0 \\
-d'(w)d(w)\sigma^2(w) + \sigma'(w)\sigma(w)d^2(w) &\geq 0 \\
-d'(w)\sigma(w) + \sigma'(w)d(w) &\geq 0
\end{aligned} \tag{16}$$

Where $\sigma(w) = [(1+w)^2 + w^2]^{\frac{1}{2}}$, $d(w) = \Delta_1 + \Delta + w(\Delta_1 - \Delta_2)$. Let $D = (1+w)^2 + w^2$, $f = \Delta_1 + \Delta$, $C = \Delta_1 - \Delta_2$. Then,

$$\begin{aligned}
D^{-\frac{1}{2}}(2w+1)[\Delta_1 + \Delta + wC] - CD^{\frac{1}{2}} &\geq 0 \\
[2w+1](f+wC) - C[2w^2+2w+1] &\geq 0 \\
[2f-C]w + f - C &\geq 0 \\
[2(\Delta_1 + \Delta) - (\Delta_1 - \Delta_2)]w + (\Delta + \Delta_2) &\geq 0 \\
(2\Delta + \Delta_2 + \Delta_1)w + \Delta + \Delta_2 &\geq 0 \\
(2\Delta + \Delta_2 + \Delta_1)w &\geq -(\Delta + \Delta_2)
\end{aligned} \tag{17}$$

Thus,

if $2\Delta + \Delta_1 + \Delta_2 > 0$, the function $I(w)$ is monotonically increasing when $w \geq -\frac{\Delta + \Delta_2}{2\Delta + \Delta_2 + \Delta_1}$;

if $2\Delta + \Delta_1 + \Delta_2 < 0$, the function $I(w)$ is monotonically increasing when $w \leq -\frac{\Delta + \Delta_2}{2\Delta + \Delta_2 + \Delta_1}$;

if $2\Delta + \Delta_1 + \Delta_2 = 0$, the function $I(w)$ is monotonically increasing regardless of the value of w .

(2) When $x_a < 0$, that is $d(w) < 0$.

Similarly, we can obtain,

if $2\Delta + \Delta_1 + \Delta_2 > 0$, the function $I(w)$ is monotonically increasing when $w \leq -\frac{\Delta + \Delta_2}{2\Delta + \Delta_2 + \Delta_1}$;

if $2\Delta + \Delta_1 + \Delta_2 < 0$, the function $I(w)$ is monotonically increasing when $w \geq -\frac{\Delta + \Delta_2}{2\Delta + \Delta_2 + \Delta_1}$;

if $2\Delta + \Delta_1 + \Delta_2 = 0$, the function $I(w)$ is monotonically increasing regardless of the value of the parameter w .

Next focus on $-\frac{\Delta + \Delta_2}{2\Delta + \Delta_2 + \Delta_1}$, let $\Delta_1 - \Delta_2 = h(\Delta + \Delta_2)$.

$$\begin{aligned}
-\frac{\Delta + \Delta_2}{2\Delta + \Delta_2 + \Delta_1} &= -\frac{1}{2 + \frac{b}{\Delta + \Delta_2}} \\
&= -\frac{1}{2 + \frac{h(\Delta + \Delta_2)}{\Delta + \Delta_2}} \\
&= -\frac{1}{2 + h}
\end{aligned} \tag{18}$$

Neural network in the training process $\varepsilon_\theta(x_t, y, t)$, $\varepsilon_\theta(x_t, t)$ using the same set of network structure, and in the code practice, both of them are the same super parameter. Thus $\Delta_1 - \Delta_2$ is small, and then h is the small value whose positive or negative cannot be determined. But the n value, being very small, does not affect the overall $-\frac{\Delta + \Delta_2}{2\Delta + \Delta_2 + \Delta_1}$ positively or negatively.

$$-\frac{\Delta + \Delta_2}{2\Delta + \Delta_2 + \Delta_1} = -\frac{1}{2+n} < 0 \quad (19)$$

When $2\Delta + \Delta_1 + \Delta_2 > 0$ and $d > 0, w > 0$ increasing can improve the robustness of the conditional diffusion model. However, if increasing $2\Delta + \Delta_1 + \Delta_2 < 0$ and $d > 0, w > 0$ increasing does not improve the robustness of the conditional diffusion model. The analysis of all the situations are summarized in Figure A.2.

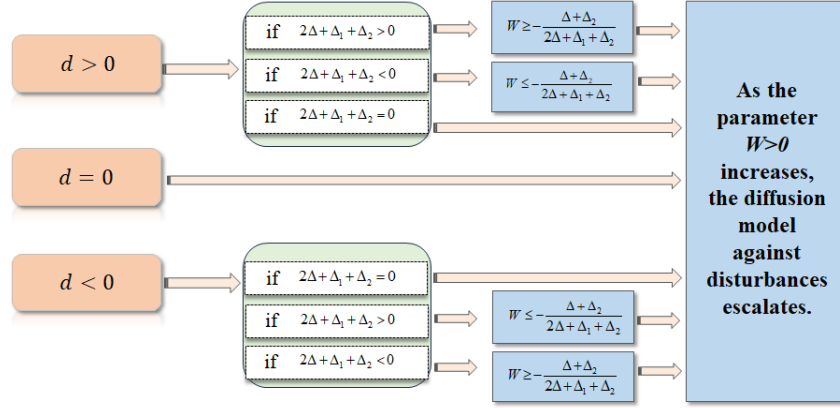


Figure A.2: Situation analysis

In simple terms, when Δ is sufficiently large or small, the $2\Delta + \Delta_1 + \Delta_2$ matches that of Δ . It leads to the conclusion that if $\Delta > 0$, as long as $d \geq 0$, increasing the parameter w enhances the robustness of the diffusion model against interference. Similarly, if $\Delta < 0$, as long as $d \leq 0$, increasing the parameter w improves the model's resistance to interference. Therefore, we only need to consider the d in different scenarios with varying Δ . Where Δ_2 and Δ_1 are variables that vary within the range of $[-c, c]$.

(1) $\Delta > 0$

$$\begin{aligned} d &= (1+w)\Delta_1 - w\Delta_2 + \Delta \geq 0 \\ [(1+w)\Delta_1 - w\Delta_2 + \Delta]_{min} &\geq 0 \\ [-c(1+2w) + \Delta] &\geq 0 \\ w &\leq \frac{\Delta}{2c} - \frac{1}{2} \end{aligned} \quad (20)$$

When $\Delta > 0$ and is sufficiently large, within the range of $[0, \frac{\Delta}{2c} - \frac{1}{2}]$, the function $I(w)$ monotonically increases as the parameter w increases.

(2) $\Delta < 0$

$$\begin{aligned} d &= (1+w)\Delta_1 - w\Delta_2 + \Delta \leq 0 \\ [(1+w)\Delta_1 - w\Delta_2 + \Delta]_{max} &\leq 0 \\ [c(1+2w) + \Delta] &\leq 0 \\ w &\leq -\frac{\Delta}{2c} - \frac{1}{2} \end{aligned} \quad (21)$$

When $\Delta < 0$ and is sufficiently large, within the range of $[0, -\frac{\Delta}{2c} - \frac{1}{2}]$, the function $I(w)$ monotonically increases as the w increases.

In summary, the function $I(w)$ must be monotonically increasing in the range $[0, \frac{|\Delta|}{2c} - \frac{1}{2}]$.

A.3.4 Proof for Lemma 3.3

Let the random variable $a = (1+w)\Delta_1$ with $a \in [-(1+w)c, (1+w)c]$, and $b = w\Delta_2$ with $b \in [-wc, wc]$, where Δ_1 and Δ_2 are independent variables within the range of $[-c, c]$. Then the

probability density function $p(d)$ of $d(w) = (1 + w)\Delta_1 - w\Delta_2 + \Delta$ can be solved as follows.

$$p(d) = \begin{cases} \frac{2cw+c+d}{4c^2w(w+1)} & \text{if } -2cw - c + \Delta \leq d \leq -c + \Delta, \\ \frac{1}{2c(w+1)} & \text{if } -c + \Delta \leq d \leq c + \Delta, \\ \frac{2cw+c-d}{4c^2w(w+1)} & \text{if } c + \Delta \leq d \leq 2cw + c + \Delta. \end{cases} \quad (22)$$

Under different values of Δ , the probability density function $p(d|w)$ exhibits sensitivity to w . Specifically, when w takes the values of $\frac{n|\Delta|}{2c} - \frac{1}{2}$ and $\frac{\Delta}{2c} - \frac{1}{2}$, respectively, we have illustrated the trend of $p(d|w)$ through graphical representations. The specific changes of $p(d|w)$ are shown in Figure A.3.

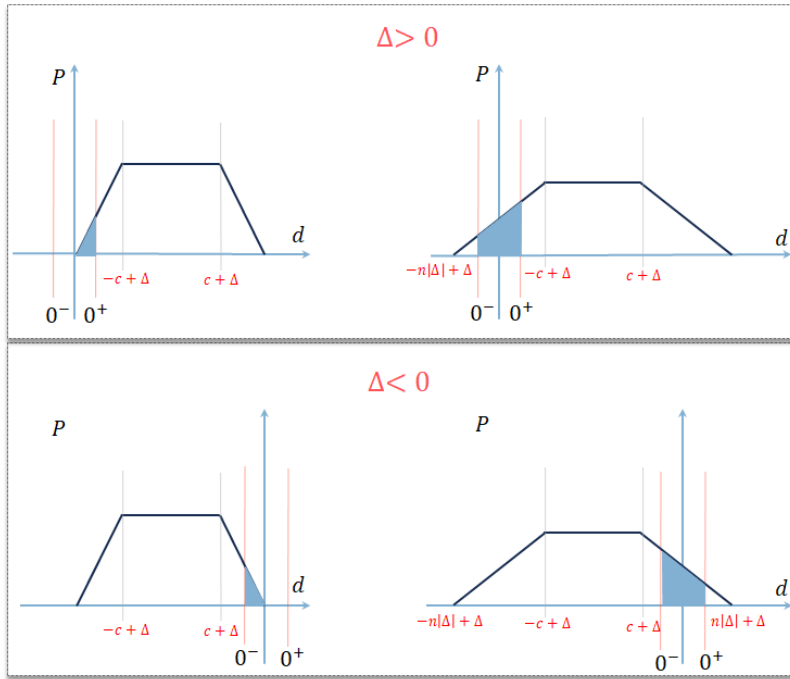


Figure A.3: Schematic of balance factor n role

The increase of the balance factor n significantly affects the function $d(w)$. When $\Delta > 0$, the variable $d(w)$ still has a high probability of satisfying $d(w) \geq 0$ as n increases. When $\Delta < 0$, $d(w)$ still has a high probability of satisfying $d(w) \leq 0$. Additionally, increasing n allows $d(w)$ to maintain a certain probability near zero. This adjustment effectively balances the fulfillment of function value constraints and the maintenance of monotonic.

A.4 Experimental Results

A.4.1 Extended Results on MNIST Dataset

Herein, we present the experimental outcomes from Section 4.1 in detail as a supplement to the results discussed in the main paper. Figures A.4~A.5 illustrate the results and provide visual evidence of the phenomena observed during the experiments.

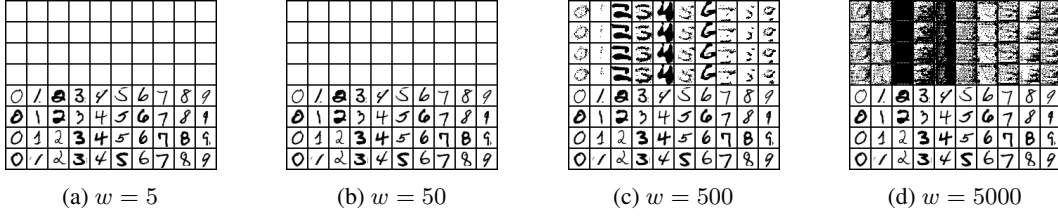


Figure A.4: Reflections of $\Delta = 3$ on different values of w . With $w = 500$, the model can generate numbers in the presence of errors.

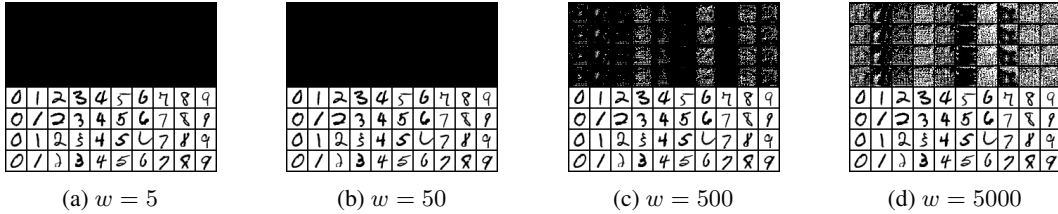


Figure A.5: Reflections of $\Delta = -3$ on different values of w .

A.4.2 Extended Results on CIFAR-10 Dataset

To ensure the comprehensiveness and transparency of this paper, following the detailed descriptions of our experimental design, procedures, and key findings, we provide supplementary graphical materials in this section. These materials include comparative visualizations across various network structures, the effectiveness of different sampling methods, and the impact of varying w values under different error conditions.

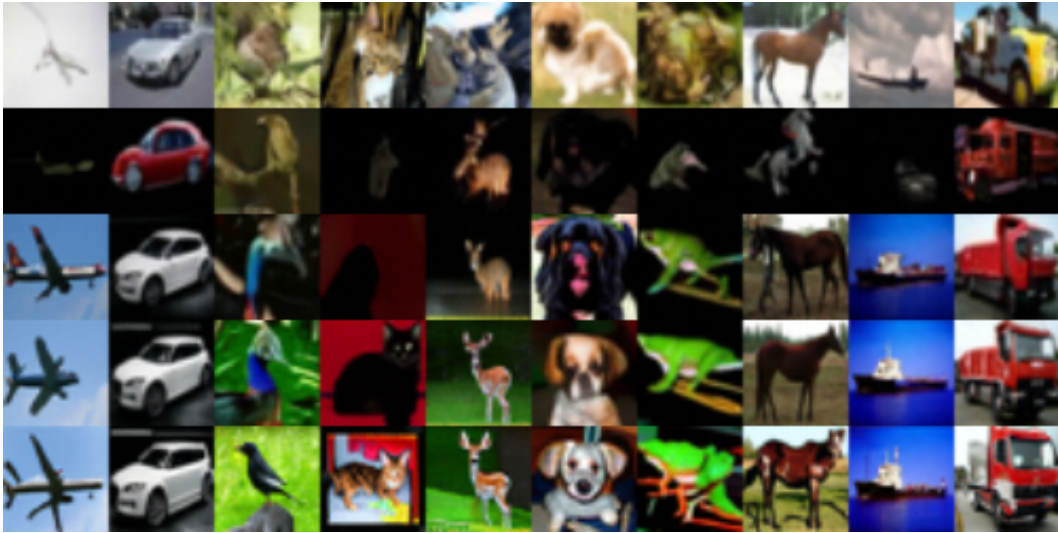


Figure A.6: Visualization of the final generation results in $\Delta = 0.03$, DDPM and U-vit on CIFAR-10 dataset. The top row of the image illustrates the ideal state where the CDM generates images without any error. Subsequent 2~5 rows, demonstrate the images produced by RCDM with the w set to 0, 5, 10, and 20, respectively.

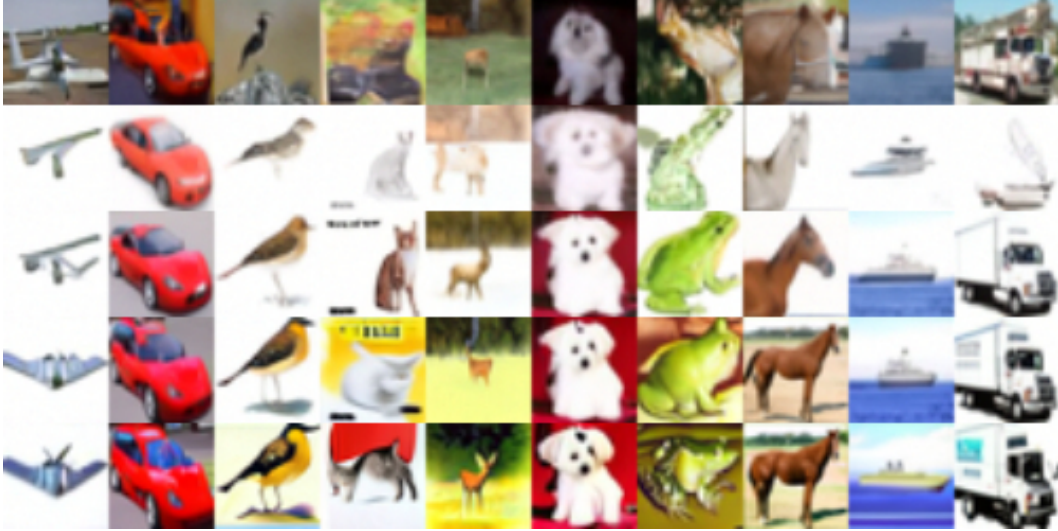


Figure A.7: Visualization of the final generation results in $\Delta = -0.03$, DDIM and U-net on CIFAR-10 dataset. The top row of the image illustrates the ideal state where CDM generates images without any error. Subsequent 2~5 rows, demonstrate the images produced by RCDM with w set to 0, 5, 10, and 20, respectively.

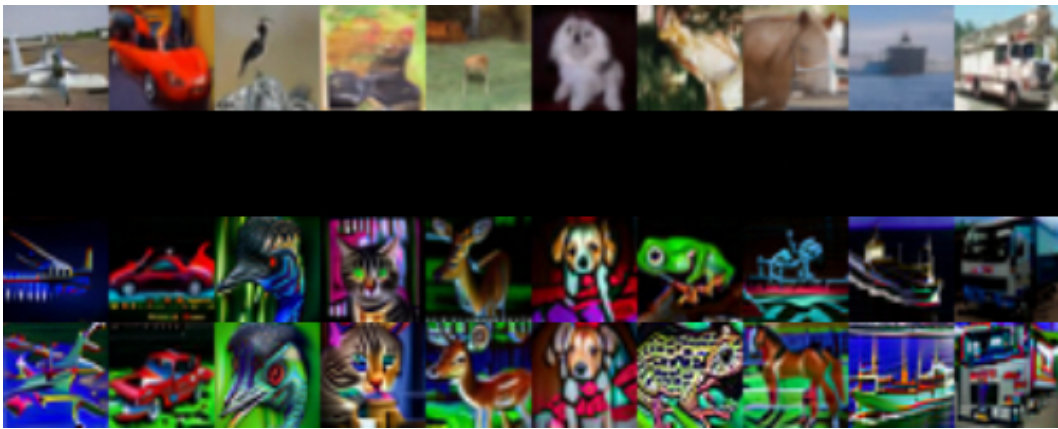


Figure A.8: Visualization of the final generation results in $\Delta = 0.3$, DDPM and U-net on CIFAR-10 dataset. The top row of the image illustrates the ideal state where CDM generates images without any error. Subsequent 2~4 rows, demonstrate the images produced by RCDM with w set to 0, 50, and 100, respectively.

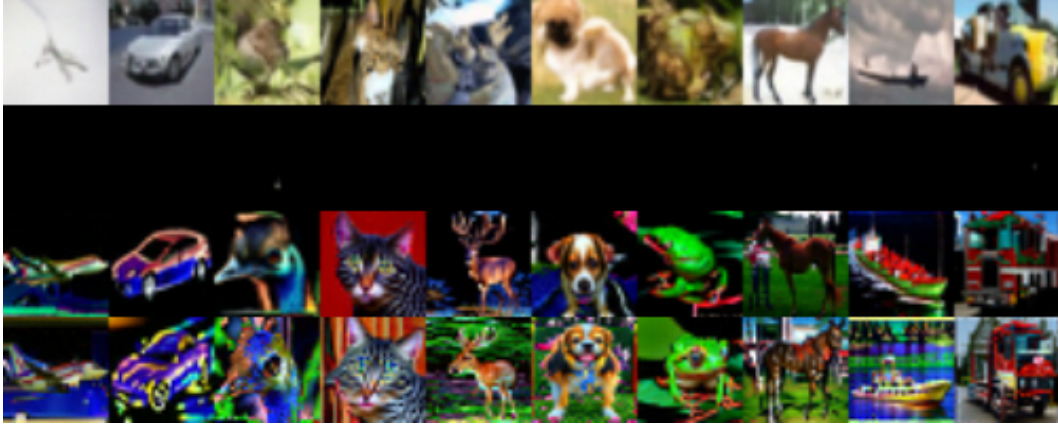


Figure A.9: Visualization of the final generation results in $\Delta = 0.3$, **DDPM** and **U-vit** on CIFAR-10 dataset. The top row of the image illustrates the ideal state where CDM generates images without any error. Subsequent 2~4 rows, demonstrate the images produced by RCDM with w set to 0, 50, and 100, respectively.

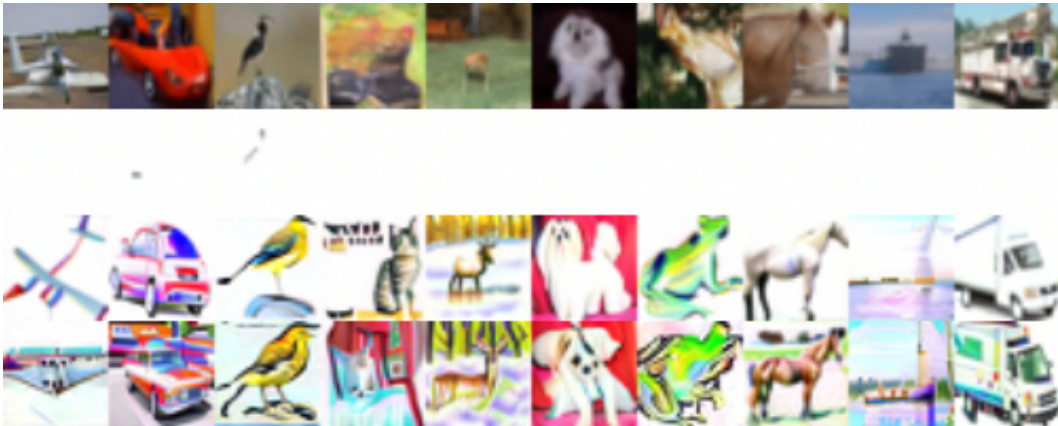


Figure A.10: Visualization of the final generation results in $\Delta = -0.3$, **DDIM** and **U-net** on CIFAR-10 dataset. The top row of the image illustrates the ideal state where CDM generates images without any error. Subsequent 2~4 rows, demonstrate the images produced by RCDM with w set to 0, 50, and 100, respectively.



Figure A.11: Visualization of the final generation results in $\Delta = -0.3$, DDIM and U-vit on CIFAR-10 dataset. The top row of the image illustrates the ideal state where CDM generates images without any error. Subsequent 2~4 rows, demonstrate the images produced by RCDM with w set to 0, 50, and 100, respectively.

A.5 Limitations

While the advancements in RCDM have provided some resistance to errors for generative tasks. However, there are several intrinsic challenges and limitations that need to be addressed. These challenges not only pertain to the technical aspects of model development but also to the practical considerations of deploying these models in real-world applications. These include refining the quantification of input errors, addressing the impact of stochastic noise, and balancing the trade-off between output diversity and model robustness. In image generation, bolstering network robustness might reduce output diversity, which could impair the task's goal of variety. However, this trade-off may be tolerable in prediction tasks where diversity is less crucial.

A.6 Broader Impact

Advancements in robust conditional diffusion models offer significant advantages. Firstly, these models are capable of dynamically adjusting w based on errors, enhancing their robustness. Secondly, they have practical implications for improving the usability and generalization of conditional diffusion models. The potential for societal impact is substantial, as these models can reshape access to high-quality generative AI, lower computational barriers, and drive innovation across creative disciplines. Ethical guidelines and verification methods are essential to ensure the technology's positive contributions, prevent misuse, and foster new job opportunities centered around AI-assisted creativity. Balancing these aspects is key to enabling the technology's constructive influence on various sectors and the broader community.

A.7 Safeguards

We are dedicated to safeguarding the personal information with robust encryption and stringent access controls, ensuring the data remains secure and confidential. Our commitment to global data protection standards and continuous security enhancements upholds the trust you place in us.